Journal of Marine Science and Technology (2019) 24:673–685
https://doi.org/10.1007/s00773-018-0577-8

ORIGINAL ARTICLE

AUV docking based on USBL navigation and vision guidance

Shuangshuang Fan[1] · Chenzhan Liu[1] · Bo Li[1] · Yuanxin Xu[1] · Wen Xu[1]

Received: 12 July 2016 / Accepted: 2 July 2018 / Published online: 3 August 2018

Abstract
Underwater docking technology makes the long-term, on-station vehicle deployment possible, which can effectively save the recovery cost and ease the operational burden. To perform docking mission, autonomous underwater vehicle (AUV) should have the capability to guide, navigate, and control itself into the docking station in a strategic manner. The navigation and guidance issues of AUV docking are addressed in the paper. Ultrashort baseline-based (USBL-based) navigation method is applied to home the vehicle to the dock station in relative long range. An integrated navigation algorithm based on extended Kalman filter (EKF) is studied, which takes acoustic outlier rejection into consideration. The software of navigation algorithm is implemented using Mission Oriented Operating Suite-Interval Programming (MOOS-IvP). Both the pool and lake tests are conducted to validate the proposed navigation system. Since the USBL sonar system can hardly navigate the vehicle entering the dock entrance with its error-bounded positioning accuracy, the more accurate vision guidance method is adopted instead of USBL navigation for terminal guidance. The combined performance of EKF navigation and vision guidance is validated by docking experiments. The experimental results demonstrate the effectiveness of the vision system for terminal guidance in spite of the bounded USBL positioning error.

Keywords Underwater docking · USBL navigation · EKF · Vision guidance · Docking experiment

1 Introduction

Autonomous underwater vehicles (AUVs) are playing an increasingly important role in ocean observation. During their missions, AUVs often carry sophisticated, but power-intensive instrumentation to sample underwater environments. However, the high-power draw of the instrumentation limits an AUV to endurance of roughly 1 day [1]. To deal with this, the conventional practice is to recover the vehicle and recharge it on shore or on a support vessel, which is not only a waste of cost and labor, but even unsafe in high sea states. Then, underwater docking concept is proposed to meet the goal of long-term, on-station vehicle deployment [2]. The docking node or station is designed to link to the power and communication infrastructure of a mooring or a cabled observatory node, enabling the AUV to operate independently of the artificial recovery for extended periods. While docked, the AUV can recharge its batteries, upload observation data, download new instructions, and safely park until the next mission, which also help to capture the interesting oceanographic phenomenon promptly.

To fulfill this idea, advances in the state-of-the-art of dock and vehicle design as well as the effective target tracking capability of the vehicle are all essential to docking mission [3]. Underwater tracking missions require a lot on vehicle sensing and maneuvering [4–6]. For a fundamental successful docking operation, the AUV is required to be able to guide, navigate, and control itself into the docking station in a strategic manner, depending on docking scenario and homing sensor type [7].

As a promising technology, AUV docking system has been studied for more than 2 decades by many groups around the world. Based on different navigation and guidance devices, several kinds of navigation and guidance methods have been proposed for underwater docking, including optical terminal guidance [8, 9], camera vision guidance [10, 11], electromagnetic homing [12], acoustic positioning using short baseline (SBL) system [13, 14], and ultrashort baseline (USBL) system [1, 15]. While each

✉ Yuanxin Xu
xuyx@zju.edu.cn

Shuangshuang Fan
ssfan@zju.edu.cn

[1] College of Information Science and Electronic Engineering, Zhejiang University, Hangzhou 310027, China

type has its own pros and cons, USBL sonar system can provide error-bounded position fix and has the advantage of positioning in relative large range, which is also mature and commercially available; on the other hand, camera vision system can implement accurate terminal guidance in short range, which is simple and effective in practice. For these reasons, we combine the above two techniques, applying the USBL sonar system for long-ranged navigation and the camera vision system for terminal guidance throughout the docking mission.

Integrated navigation based on Bayesian filter is widely used for multiple sensor data fusion of AUV, to improve navigation accuracy and feed continuous navigation data to motion controllers. Kalman filter (KF) is a popular sequential Bayesian filtering algorithm for linear system; however, the AUV is a nonlinear dynamic system, where the Kalman filter no longer works well [16]. For nonlinear systems, it is difficult or even impossible to obtain the exact optimal filtering solution due to the infinite integral operation [17], so that a large number of sub-optimal approximate nonlinear filtering algorithms are proposed, such as extended Kalman filter (EKF), unscented Kalman filter (UKF), cubature Kalman filter (CKF), particle filter (PF), and so on [18, 19]. With a trade-off between accuracy and complexity, we adopt the EKF algorithm for AUV navigation.

To extend the existing research achievement, our work in this paper includes the following main contributions: outlier rejection issue related to acoustic measurements is carefully addressed to make the integrated navigation algorithm based on EKF applied properly. The proposed navigation algorithm is implemented using Mission Oriented Operating Suite-Interval Programming (MOOS-IvP) and further validated by field trials. Due to the error-bounded positioning accuracy of the USBL navigation system, which is confirmed by the field trial data, a simple vision guidance system is adopted to ensure reliable terminal docking operation. An experimental method is proposed to demonstrate the position-error tolerance of the vision guidance system. Overall, this paper aims to address the essential navigation and guidance issues in AUV docking processes. The feasible methods and scheme are presented to counter the abnormal and less accurate navigation data.

The rest of the paper is organized as follows. Section 2 introduces our underwater docking system as well as the docking scheme. In Sect. 3, we discuss the USBL-based navigation method in detail, including the integrated navigation algorithm, the software implementation with MOOS-IvP, and the outlier detection and removal method, as well as the performance validation of the proposed navigation system. Due to the error-bounded positioning accuracy of the USBL navigation system, the vision terminal guidance method is further presented in Sect. 4, together with the experimental method and results of AUV terminal docking operation. Section 5 summarizes the main contributions and describes some additional avenues for continuing research.

2 Underwater docking system and scheme

2.1 Docking system overview

A small-sized, modular AUV for underwater environmental sampling has been developed at Zhejiang University, called Dolphin II. The AUV has a modular mechanical, electronic, and software design which allows for a simple integration of payload sensors for different applications [20]. For docking mission, the vehicle consists of five sections, from bow to stern, which are camera and USBL sonar transceiver section, data and power transmission section, battery and control section, navigation and communication section, and propulsion and steering section, respectively. The nose cap of the AUV is made of polycarbonate, a material that is acoustically and optically transparent. The Dolphin II AUV is under-actuated with a propeller in the tail for propulsion and four identical tail fins arranged in an X-typed configuration for attitude steering.

The vehicle can dock with a special-designed docking station, which can be cabled to a seafloor observatory node. Since then, the docking station can provide limitless power for the vehicle and communicate with it for information interaction. The docking station has a funnel-shaped entrance that helps to guide the vehicle into the dock passively; in addition, the docked AUV can be protected in the tube from environmental disturbances. The shape of the funnel has an important impact on AUV docking operation; in our case, the funnel-shaped entrance has a diameter of 1.1 m and a cone angle of 60°. When the AUV enters the docking station, it will be clamped by a gripper for stable data and power transmission, while the gripper is made of three electromagnets for the purpose of simplicity and reliability. An acoustic beacon is mounted on the frame of the docking station, aiming to home the vehicle toward the dock entrance, while an underwater light is also fixed on the dock frame, but it is aligned with the centerline of the dock entrance. More details of the docking station can be found in [21].

Our AUV docking system is shown in Fig. 1. In our system, both the USBL sonar system and the acoustic beacon are products from EvoLogics [22]. Using this pair of inductors, the position of the vehicle relative to the dock can be sensed for vehicle navigation. While both the camera and the underwater LED light come from Outland Technology, which are used for terminal vision guidance during AUV docking process [23].

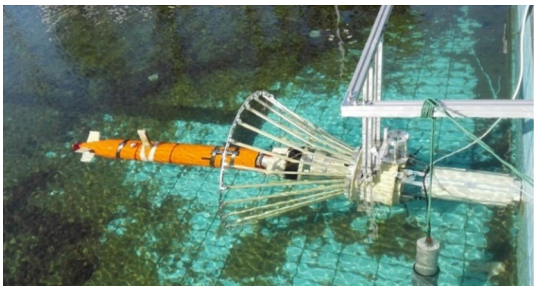

Fig. 1 AUV docking system

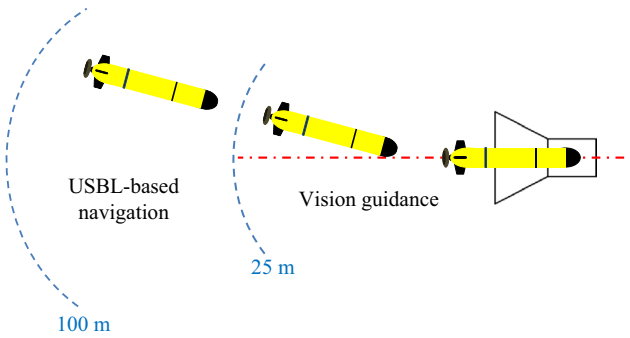

Fig. 2 Schematic illustration of docking scheme

2.2 Docking scheme considerations

Docking scheme depends on the performance of homing sensors either for navigation or guidance. Due to the performance features of the USBL navigation system and the vision guidance system, our docking scheme is divided into two steps: long-ranged homing and short-ranged docking; see Fig. 2.

When the AUV is far from the dock, which is beyond the work range of USBL sonar system, autonomous navigation is implemented to navigate the vehicle running toward the dock, with commonly used navigation devices, such as global positioning system (GPS), inertial navigation system (INS), Doppler velocity log (DVL), electronic compass, depth sensor or altimeter, and so on. As the vehicle gets close to the dock, usually within the range of 100 m, the USBL sonar system can provide stable position fix, which can be used for vehicle navigation; at this time, the vehicle enters the USBL-based navigation stage. With the navigation feedback information, motion controller will transit the vehicle to a fixed approaching path, much like an airplane landing on a runway. In fact, the USBL sonar transceiver can obtain the bearing information with respect to the acoustic beacon earlier than the position fix. The bearing information can be used for pure pursuit guidance, which is implemented to keep the vehicle's nose continuously pointing at the beacon for increasing signal strength. While we will not discuss this process in this paper, one can refer to [1, 24] for more details.

With USBL-based navigation, the vehicle can only be navigated close to the dock, but cannot enter the dock entrance accurately. That is because the accuracy of USBL-based navigation during AUV dynamical flight is unable to meet the requirement for exact docking operation. For successful docking, the positioning accuracy of vehicle navigation should be much less than 0.55 m, which is confined by the dimension of the dock entrance. In this case, we resort to camera vision system for accurate terminal guidance when the vehicle is less than 25 m far away from the dock. Vision guidance aims to maintain the image of the light at the center of the field-of-view of the camera by vehicle maneuvering, so that the AUV nose can be kept pointing at the light even without position feedback. Thus, with the combination of both the USBL-based navigation and vision guidance algorithms, the vehicle can be navigated and guided into the dock entrance gradually.

3 USBL-based navigation method

We choose an USBL sonar as the transceiver mounted in the vehicle nose and an acoustic beacon as the transponder fixed at the frame of the docking station. Using this pair of inductors, the position of the vehicle relative to the dock can be sensed. However, the updating rate of the USBL position fix is usually lower than 0.5 Hz, which is hard to provide continuously feedback data for motion control. In spite of USBL sonar system, the vehicle is also equipped with various commonly used devices for autonomous navigation. In such conditions, it is quite necessary to apply some integrated navigation algorithm, not only for multiple data fusion and increase of navigation accuracy, but also to feed continuous navigation data to motion controllers.

The integrated navigation algorithm fuses the multiple sensor measurements by sequential Bayesian filtering, to estimate the motion state of the vehicle. The basic principle of sequential Bayesian filtering is to set up the system and measurement models first; and then use filtering algorithm to obtain the optimal estimation of system state, which is capable of reducing the interference of measurement noise and improving the navigation accuracy [25].

3.1 Integrated navigation algorithm

3.1.1 Navigation model setup

There are two reference frames that are necessary to be established for the navigation model setup. One is the inertial reference frame which is represented by an orthonormal triad $\{\boldsymbol{i}_1, \boldsymbol{i}_2, \boldsymbol{i}_3\}$ fixed in inertial space, where $\boldsymbol{i}_3$ is

aligned with the local direction of gravity. The other one is the body-fixed reference frame that is defined by an orthonormal triad $\{\boldsymbol{b}_1, \boldsymbol{b}_2, \boldsymbol{b}_3\}$, where $\boldsymbol{b}_1$ is aligned with the body's longitudinal axis. The origin of the body frame sits at the vehicle's center of buoyancy; see Fig. 3.

Let $\boldsymbol{X} = [x, y, z]^T$ represent the position vector from the origin of the inertial frame to the origin of the body frame. The vector $\boldsymbol{X}$ is the North-East-Down coordinates, expressed in the inertial frame. To facilitate the following discussion, we let $\boldsymbol{\Theta} = [\varphi, \theta, \psi]^T$ represent the "attitude vector", which is expressed by Euler angles, that is: the roll angle φ, the pitch angle θ, and the yaw angle ψ. Besides, let $\boldsymbol{v} = [u, v, w]^T$ and $\boldsymbol{\omega} = [p, q, r]^T$, respectively, represent the translational and rotational velocity of the vehicle with respect to the inertial frame, but expressed in the body frame. The kinematic equations are as follows:

$$\begin{aligned} \dot{\boldsymbol{X}} &= \boldsymbol{R}_{\mathrm{IB}}\boldsymbol{v}, \\ \dot{\boldsymbol{\Theta}} &= \boldsymbol{L}_{\mathrm{IB}}\boldsymbol{\omega}, \end{aligned} \tag{1}$$

where $\boldsymbol{R}_{\mathrm{IB}}$ and $\boldsymbol{L}_{\mathrm{IB}}$ are the translational and rotational rotation matrices, respectively. They are the functions of Euler angles; referring to Fossen [26], we have the following:

$$\boldsymbol{R}_{\mathrm{IB}}(\boldsymbol{\Theta}) = \begin{bmatrix} \cos\psi\cos\theta & -\sin\psi\cos\varphi + \cos\psi\sin\theta\sin\varphi & \sin\psi\sin\varphi + \cos\psi\cos\theta\sin\varphi \\ \sin\psi\cos\theta & \cos\psi\cos\varphi + \sin\psi\sin\theta\sin\varphi & -\cos\psi\sin\varphi + \sin\psi\sin\theta\cos\varphi \\ -\sin\theta & \cos\theta\sin\varphi & \cos\theta\cos\varphi \end{bmatrix}, \tag{2}$$

and

$$\boldsymbol{L}_{\mathrm{IB}}(\boldsymbol{\Theta}) = \begin{bmatrix} 1 & \sin\varphi\tan\theta & \cos\varphi\tan\theta \\ 0 & \cos\varphi & -\sin\varphi \\ 0 & \sin\varphi/\cos\theta & \cos\varphi/\cos\theta \end{bmatrix}. \tag{3}$$

Actually, AUV kinematics is continuous; however, sensor measurement is usually obtained by discrete sampling; in addition, the navigation algorithm is implemented by the digital computer of an embedded system. Hence, AUV kinematic equations are often discretized, and then, a discrete-time filtering algorithm can be applied.

We define $\mathbf{x}_k = [\,X\ Y\ Z\ u\ v\ w\ \varphi\ \theta\ \psi\,]^T$ as the state vector of the system. To reduce the dimension of the state vector, the vehicle's acceleration and angular velocity are taken as the inputs of the system; the input vector can be written as $\mathbf{u}_k = [\,\dot{u}\ \dot{v}\ \dot{w}\ p\ q\ r\,]^T$. Thus, the discrete system model is as follows:

$$\mathbf{x}_k = \begin{bmatrix} \mathbf{I}_{3\times3} & \boldsymbol{R}_{\mathrm{IB}}(\boldsymbol{\Theta}_{k-1})\Delta t & 0_{3\times3} \\ 0_{3\times3} & \mathbf{I}_{3\times3} & 0_{3\times3} \\ 0_{3\times3} & 0_{3\times3} & \mathbf{I}_{3\times3} \end{bmatrix}\mathbf{x}_{k-1} + \begin{bmatrix} 0_{3\times3} & 0_{3\times3} \\ \mathbf{I}_{3\times3} & 0_{3\times3} \\ 0_{3\times3} & \boldsymbol{L}_{\mathrm{IB}}(\boldsymbol{\Theta}_{k-1}) \end{bmatrix}\mathbf{u}_{k-1}\Delta t, \tag{4}$$

where $\mathbf{I}_{3\times3}$ represents the 3×3 identity matrix; $0_{3\times3}$ is the 3×3 matrix of zeros; k is the discrete-time index (time step); Δt denotes the time interval.

According to the functions of the vehicle's sensor suit, the vehicle's depth, attitude, and velocity can be measured by the depth sensor, electrical compass, and DVL, respectively. When the AUV runs on the surface of the water, the vehicle's position in the horizontal plane can be obtained by GPS receiver; while AUV flies underwater, the USBL position fix can be used to derive AUV position in the horizontal plane, with the dock position known in advance.

Thus, the measurement vector can be defined as $\mathbf{z}_k = [\,X\ Y\ Z\ u\ v\ w\ \varphi\ \theta\ \psi\,]^T$; then, the measurement model is as follows:

$$\mathbf{z}_k = \boldsymbol{H}\mathbf{x}_k. \tag{5}$$

No matter the AUV moves on the surface of water or underwater, the measurement matrix $\boldsymbol{H}$ can be both described by $\mathbf{I}_{9\times9}$, where $\mathbf{I}_{9\times9}$ is the 9×9 identity matrix.

To simplify the expression without losing generality, the state and measurement models can be written as the following form:

$$\begin{aligned} \mathbf{x}_k &= \boldsymbol{f}(\mathbf{x}_{k-1}) + \boldsymbol{\omega}_{k-1}, \\ \mathbf{z}_k &= \boldsymbol{h}(\mathbf{x}_k) + \boldsymbol{v}_k, \end{aligned} \tag{6}$$

where $\boldsymbol{f}(\cdot)$ is the system model and $\boldsymbol{h}(\cdot)$ is the measurement model; $\boldsymbol{\omega}_{k-1}$ and $\boldsymbol{v}_k$ are zero-mean, uncorrelated Gaussian white noise, respectively, for the system and measurement models, with $\boldsymbol{\omega}_{k-1} \sim N(0, \boldsymbol{Q}_{k-1})$ and $\boldsymbol{v}_k \sim N(0, \boldsymbol{R}_k)$. Note that the terms related to $\mathbf{u}_{k-1}$ are taken as the white noise in the above equations.

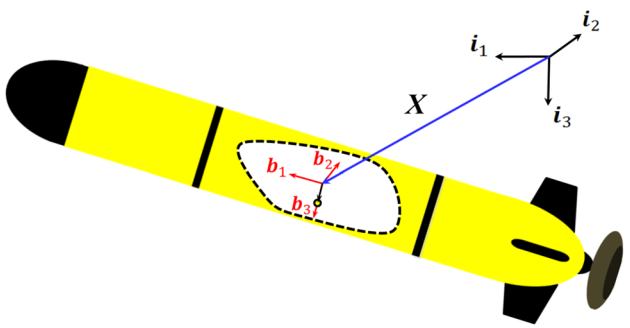

Fig. 3 Illustration of reference frames

3.1.2 Sequential Bayesian filtering algorithm

Extended Kalman filter is a kind of linearized approximation method, which uses Taylor expansion to perform the first-order linearization on the nonlinear model, and then applies Kalman filtering algorithm to estimate system state [18]. The linearized system and measurement models are as follows:

$$\begin{aligned}\mathbf{x}_k &= \boldsymbol{f}(\hat{\mathbf{x}}_{k-1}) + \boldsymbol{F}_{k-1}(\mathbf{x}_{k-1} - \hat{\mathbf{x}}_{k-1}) + \boldsymbol{\omega}_{k-1},\\ \mathbf{z}_k &= \boldsymbol{h}(\hat{\mathbf{x}}_{k|k-1}) + \boldsymbol{H}_k(\mathbf{x}_k - \hat{\mathbf{x}}_{k|k-1}) + \boldsymbol{v}_k,\end{aligned} \tag{7}$$

where $\boldsymbol{F}_{k-1}$ is the process Jacobian matrix and $\boldsymbol{H}_k$ is the measurement Jacobian matrix:

$$\begin{aligned}\boldsymbol{F}_{k-1} &= \left.\frac{\partial \boldsymbol{f}}{\partial \mathbf{x}_{k-1}}\right|_{\mathbf{x}_{k-1} = \hat{\mathbf{x}}_{k-1}},\\ \boldsymbol{H}_k &= \left.\frac{\partial \boldsymbol{h}}{\partial \mathbf{x}_k}\right|_{\mathbf{x}_k = \hat{\mathbf{x}}_{k|k-1}}.\end{aligned} \tag{8}$$

Extended Kalman filter algorithm is recursive and implemented in two steps: forecast and update. The forecast step consists of both the state estimation and the state error covariance estimation between two sampling instants. The update step occurs at each sampling time when the sensor measurement is available to fuse and improve the accuracy of state estimation. Hence, one iteration of the EKF can be described by the following consecutive steps:

- Forecast:

$$\begin{aligned}\hat{\mathbf{x}}_{k|k-1} &= \boldsymbol{f}(\hat{\mathbf{x}}_{k-1}),\\ \boldsymbol{P}_{k|k-1} &= \boldsymbol{F}_{k-1}\boldsymbol{P}_{k-1}\boldsymbol{F}_{k-1}^T + \boldsymbol{Q}_{k-1},\end{aligned} \tag{9}$$

  where $\hat{\mathbf{x}}_{k|k-1}$ is the state forecast; $\boldsymbol{P}_{k|k-1}$ is the error covariance prediction of the state, with the last error covariance $\boldsymbol{P}_{k-1}$.
- Update:

$$\begin{aligned}\boldsymbol{K}_k &= \boldsymbol{P}_{k|k-1}\boldsymbol{H}_k^T(\boldsymbol{H}_k\boldsymbol{P}_{k|k-1}\boldsymbol{H}_k^T + \boldsymbol{R}_k)^{-1},\\ \hat{\mathbf{x}}_k &= \hat{\mathbf{x}}_{k|k-1} + \boldsymbol{K}_k(\mathbf{z}_k - \boldsymbol{h}(\hat{\mathbf{x}}_{k|k-1})),\\ \boldsymbol{P}_k &= (\mathbf{I} - \boldsymbol{K}_k\boldsymbol{H}_k)\boldsymbol{P}_{k|k-1},\end{aligned} \tag{10}$$

  where $\boldsymbol{K}_k$ is the filter gain; $\hat{\mathbf{x}}_k$ is the state update; $\boldsymbol{P}_k$ is the update of error covariance. The objective of EKF is to obtain the optimal estimation $\hat{\mathbf{x}}_k$ of the state vector $\mathbf{x}_k$ using the measurements so as to minimize the state estimation error.

3.1.3 Outlier detection and removal

Underwater environment is extremely complex, which may induce outliers among the acoustic measurements due to multipath propagation and reverberation, such as the velocity outlier of DVL and the position fix outlier of USBL [27]. Take the USBL outlier for example, spurious acoustic measurements caused by multipath propagation are inevitable, so that the acoustic travel time data may possess a certain amount of outliers. Since then, the outlier rejection issue should be carefully addressed to make sure that the EKF algorithm can be properly applied.

In the framework of Kalman filter, the measurements have effect on state estimation by the residual error:

$$\tilde{\mathbf{z}}_k = \mathbf{z}_k - \boldsymbol{h}(\hat{\mathbf{x}}_{k|k-1}). \tag{11}$$

Hence, the outlier can be detected if the residual error appears abnormal. If there is no outlier before the moment k, the forecast of measurement vector calculated by the filtering algorithm at the moment k can be considered to be accurate. Then, the residual error at the moment k will satisfy $\tilde{\mathbf{z}}_k \sim N(0, \boldsymbol{T}_k)$, where $\boldsymbol{T}_k$ is the covariance of new information at the moment k. On the contrary, if there exists some outlier in the measurement vector $\mathbf{z}_k$, the mean of the residual error will no longer be zero at the moment k. Therefore, we can make the following binary hypothesis on the residual error:

- H_0: $E[\tilde{\mathbf{z}}_k] = 0$, $E[\tilde{\mathbf{z}}_k\tilde{\mathbf{z}}_k^T] = \boldsymbol{T}_k$, there is no outlier;
- H_1: $E[\tilde{\mathbf{z}}_k] = \boldsymbol{\mu}_k$, $E[(\tilde{\mathbf{z}}_k - \boldsymbol{\mu}_k)(\tilde{\mathbf{z}}_k - \boldsymbol{\mu}_k)^T] = \boldsymbol{T}_k$, there exists outlier;

where $\boldsymbol{\mu}_k$ is the expectation of residual error $\tilde{\mathbf{z}}_k$.

Since the residual error $\tilde{\mathbf{z}}_k$ obeys Gauss distribution, the probability density function can be expressed as follows:

$$\begin{aligned}p(\tilde{\mathbf{z}}_k|H_0) &= \frac{1}{\sqrt{2\pi}|\boldsymbol{T}_k|^{1/2}}\exp\left(-\frac{1}{2}\tilde{\mathbf{z}}_k^T\boldsymbol{T}_k^{-1}\tilde{\mathbf{z}}_k\right),\\ p(\tilde{\mathbf{z}}_k|H_1) &= \frac{1}{\sqrt{2\pi}|\boldsymbol{T}_k|^{1/2}}\exp\left(-\frac{1}{2}(\tilde{\mathbf{z}}_k - \boldsymbol{\mu}_k)^T\boldsymbol{T}_k^{-1}(\tilde{\mathbf{z}}_k - \boldsymbol{\mu}_k)\right),\end{aligned} \tag{12}$$

where $|\cdot|$ denotes the determinant of a matrix.

With the following logarithmic operation:

$$\ell_k = \ln\frac{p(\tilde{\mathbf{z}}_k|\mathrm{H}_1)}{p(\tilde{\mathbf{z}}_k|\mathrm{H}_0)} \underset{\mathrm{H}_0}{\overset{\mathrm{H}_1}{\gtrless}} T_D, \tag{13}$$

we can get

$$\ell_k = \frac{1}{2}\tilde{\mathbf{z}}_k^{\mathrm{T}}\boldsymbol{T}_k^{-1}\tilde{\mathbf{z}}_k - \frac{1}{2}(\tilde{\mathbf{z}}_k - \boldsymbol{\mu}_k)^{\mathrm{T}}\boldsymbol{T}_k^{-1}(\tilde{\mathbf{z}}_k - \boldsymbol{\mu}_k). \tag{14}$$

Although in the above expression, $\boldsymbol{\mu}_k$ is unknown, it can be replaced by its maximum-likelihood estimation $\hat{\boldsymbol{\mu}}_k = \tilde{\mathbf{z}}_k$. Then, we obtain the outlier detection function:

$$\ell'_k = \tilde{\mathbf{z}}_k^{\mathrm{T}} \boldsymbol{T}_k^{-1} \tilde{\mathbf{z}}_k. \tag{15}$$

It can be proved that ℓ'_k obeys the χ^2 distribution with n_z degrees of freedom, where n_z is the dimension of the measurement vector [28]. The judgment rules for outlier detection are as follows:

- If $\ell'_k \le T_D$, $H = H_0$, there is no outlier;
- If $\ell'_k > T_D$, $H = H_1$, there exists outlier;

  where T_D is a preset threshold, which can be solved from the χ^2 distribution with given false alarm probability.

Note that if it is detected that there are outliers in the measurement vector $\mathbf{z}_k$, it does not mean that all the measurements of $\mathbf{z}_k$ are outliers. It may be the DVL velocity outlier, or USBL position outlier, or even the both. Therefore, it is better to screen out the exact rows of outliers in the measurement vector and remove them. As is already known, the outlier makes the mean of the residual error not equal to zero. Conversely, we can set each row of $\tilde{\mathbf{z}}_k$ equal to zero and compute the value of the corresponding outlier detection function, respectively; the row which makes the value of the outlier detection function minimum is identified as the row of outlier, like this:

$$i_{\text{outlier}} = \underset{i=1,2,\ldots,n_z}{\arg\min} \left(\tilde{\mathbf{z}}_k^{\mathrm{T}} \boldsymbol{T}_k^{-1} \tilde{\mathbf{z}}_k \ \text{s.t.} \ \tilde{\mathbf{z}}_k(i) = 0 \right), \tag{16}$$

where i is the row index of the residual error vector $\tilde{\mathbf{z}}_k$.

Based on the above discussion, the total process of our integrated navigation algorithm can be illustrated by Fig. 4. It is worth mentioning that the procedure of position uncertainty judgment works when there is no position measurement available, in which case, the navigation error will accumulate over time. The update of error covariance is calculated for each iteration if it is found over some preset threshold, the navigation derivation will be terminated for emergency treatment.

3.2 Software implementation with MOOS-IvP

The modular software of Dolphin II AUV is implemented based on MOOS-IvP, which is an open source collection of applications and libraries for autonomous vehicle operation [29]. An MOOS-IvP community provides a middleware capability based on a publish-subscribe architecture and protocol. Each process communicates with the others through a single database process called MOOSDB in a star-like topology. These features allow independent development of sensing, communication, and autonomous decision-making program. In addition to MOOSDB, there are various other function processes, including the pHelmIvp process for behavior coordination, the pMarinePID process for motion control, the pNav process for navigation, and so on. More details can be found in Benjamin et al. [30].

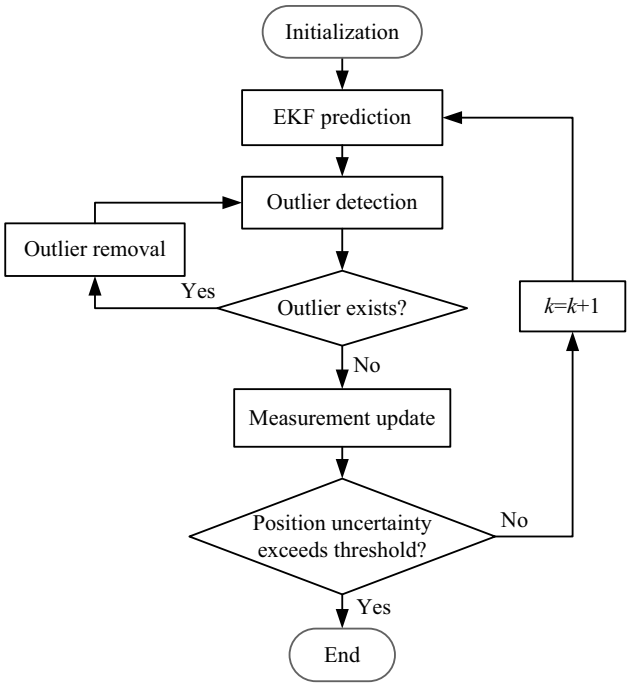

Fig. 4 Flowchart of EKF algorithm

Our navigation system based on MOOS-IvP can be visually displayed in a layered structure, from top to bottom, respectively, named as: Navigation Algorithm Layer, Data Exchange Layer, Device Interaction Layer, and Physical Device Layer; see Fig. 5. Processes with prefix "i" are called interface applications, which interact with the external devices, such as iGPS and iDVL, while processes with prefix "p" are called pure applications, which process the data acquired from MOOSDB, such as pNav. The EKF algorithm is implemented by the pNav process to derive vehicle's motion states. Although the MOOS-IvP software suite provides the pNav application, we have made some necessary modifications and improvements according to our actual demands, such as outlier rejection and position uncertainty judgment.

In Fig. 5, the processes with dashed borders are applications contained in the MOOS-IvP software suite which are publicly available from the website [31], while the other ones are processes developed or modified for our platform specially. Take the iUSBL process for example, it is designed according to the specifications of the USBL sonar system from Evologics, whose functions are as follows:

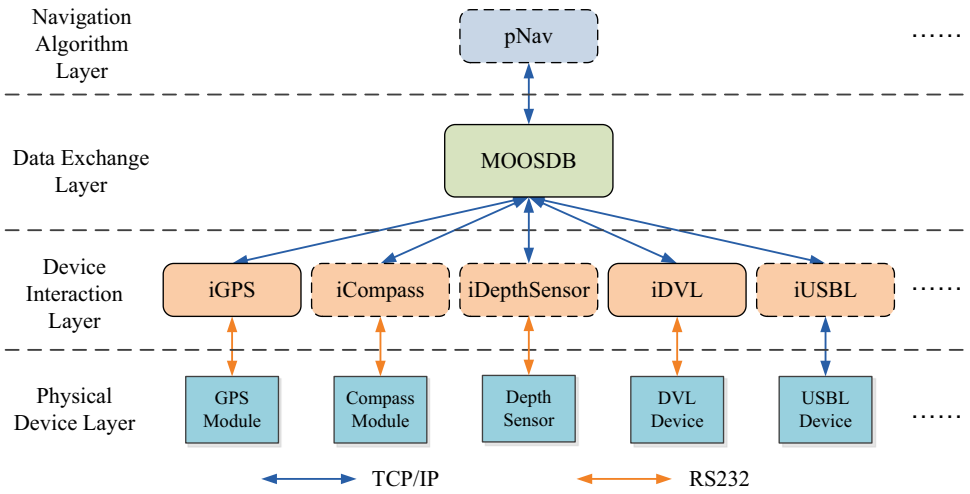

Fig. 5 Layered structure of navigation system. Blue and orange double-headed arrows denote the TCP/IP and RS232 communication interfaces, respectively. (Color figure online)

- USBL positioning data reading and parsing;
- Reporting vehicle running status and motion states to dock station;
- Receiving data or commands from dock station;
- Setting up communication connection automatically if disconnects.

3.3 Performance validation of navigation system

Both the pool and lake tests are carried out to validate the proposed navigation system, with different testing considerations.

3.3.1 Pool test

To have an intuitive understanding of AUV docking operation, docking experiments in the pool are preliminarily conducted on the surface of water, as is shown in Fig. 1. The pool is 50 m long, 21 m wide, and 1.5 m deep; the depth of water is almost 1 m. The long side has an included angle of 20° with respect to the north direction; see Fig. 6. Although the pool environment is not good for USBL positioning, as the size and orientation of the pool are known, it can provide absolute position reference for vehicle navigation.

The dock is located at the middle of one wide side of the pool, where is taken as the origin of the inertial frame; thus, the initial position for EKF derivation can be relatively accurately obtained with the measurable pool. The vehicle starts from the opposite side of the dock with forward direction parallel to the dock centerline and an initial lateral deviation of 2.5 m with respect to the dock centerline, attempting to enter the dock entrance under closed-loop control. During the docking mission, the navigation system derives the vehicle's motion states for feedback control.

Figure 7 shows the EKF navigation results compared with GPS data during a docking mission. Since the accuracy of

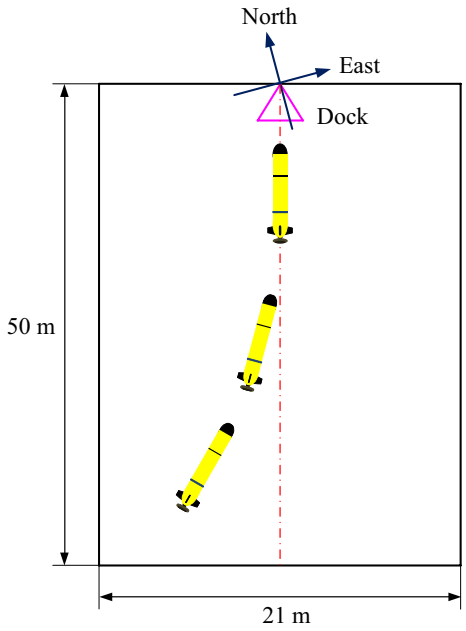

Fig. 6 Illustration of AUV docking operation with EKF navigation in the pool

GPS data is about 10 m, it cannot meet the accurate navigation requirement for docking operation (see the blue curve in Fig. 7), which is much less than 0.55 m confined by the size of dock entrance; in addition, GPS cannot work for underwater docking. For the first 20 m flight, the USBL position fix was not set to fuse into the EKF; there was some noticeable discrepancy between the EKF trajectory and the USBL position fixes, as the green curve and the red circles show in Fig. 7; after that, the EKF algorithm integrated the USBL position fix for navigation derivation, which caused a dramatic turning on the green curve. Before that moment, the vehicle was actually deviated from the dock centerline;

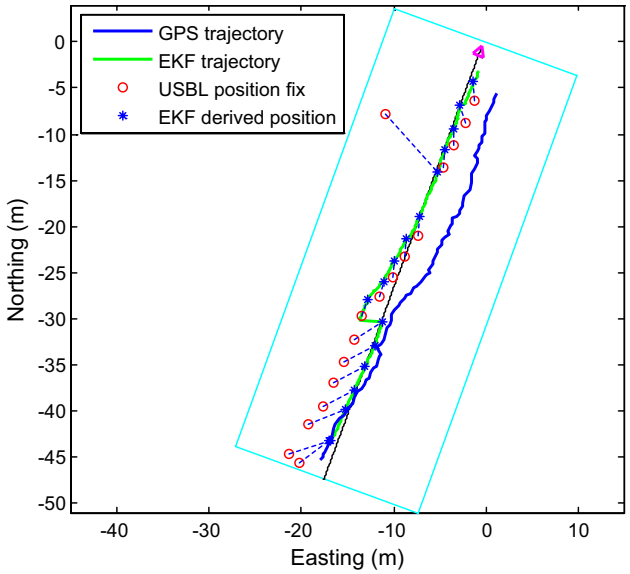

Fig. 7 EKF navigation results compared with GPS. Magenta triangle indicates the dock entrance; black line in the middle is the dock centerline; cyan rectangular box denotes the four edges of the pool. Blue asterisk indicates AUV's current position when USBL fix is available; red circle presents USBL position fix; blue dashed line connects USBL position fix with the corresponding position derived by EKF. (Color figure online)

after that, with the relatively accurate position feedback, the motion controllers were able to maneuver the vehicle to approach the dock centerline.

In our study, the false alarm probability is set to be 0.5%; since the vehicle moves in the horizontal plane, the dimension of the measurement vector is equal to 5. Look up Chi-square distribution table, the outlier detection threshold could be determined as 16.75. Note that there was an obvious USBL outlier as the vehicle ran close to the dock, while our EKF algorithm had it rejected successfully, as the green curve remains the original trend without any significant fluctuations. However, the vehicle still failed to enter the dock entrance and deviated more than 1 m from the dock centerline as observed. We owed this result to the bounded error of USBL position fix, which cannot meet the requirement for accurate docking navigation. We will further demonstrate this in later section. Nevertheless, the feasibility and effectiveness of our navigation system were validated by the pool test, except for the performance limitation of the USBL sonar system.

3.3.2 Lake test

To confirm the positioning accuracy of the USBL sonar system, we carried out a series of positioning performance tests in the Mogan Lake, Zhejiang Province, China; see Fig. 8.

Fig. 8 USBL positioning test in Mogan Lake

The lake has a relative flat bottom with the water depth of about 20 m.

Both the static and dynamic tests were conducted. During the static test, both the USBL sonar and the acoustic beacon were fixed at 5 m water depth using rigid frames. We adopted the measurements of a laser range finder as the position reference, whose accuracy is within 2 mm. The range between the USBL sonar and the acoustic beacon was respectively set as 7, 14, 19, 24, and 29 m, which was determined by the structure and size of the experimental platform anchored in the lake; see Fig. 9. The results of the tests indicated that the static positioning accuracy of the USBL system could be much less than 5 cm.

During the dynamic tests, the acoustic beacon was fixed at 5 m-depth underwater using a rigid frame, while the vehicle with the USBL sonar mounted in the nose ran a parallelogram trajectory at 5 m depth and a trajectory similar to the figure of eight at 8 m depth, respectively, at a nominal speed of 1 m/s. Throughout the flights, the vehicle was navigated by EKF algorithm with the measurements of autonomous navigation devices, but not USBL sonar system; the USBL positioning data were just recorded for accuracy evaluation.

Figure 10 presents the EKF navigation results without integration of USBL position fix. While the AUV's current position when USBL position fix is available is also marked

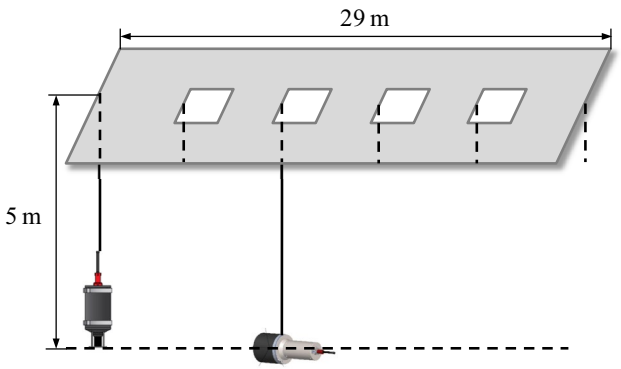

Fig. 9 Illustration of USBL static positioning test

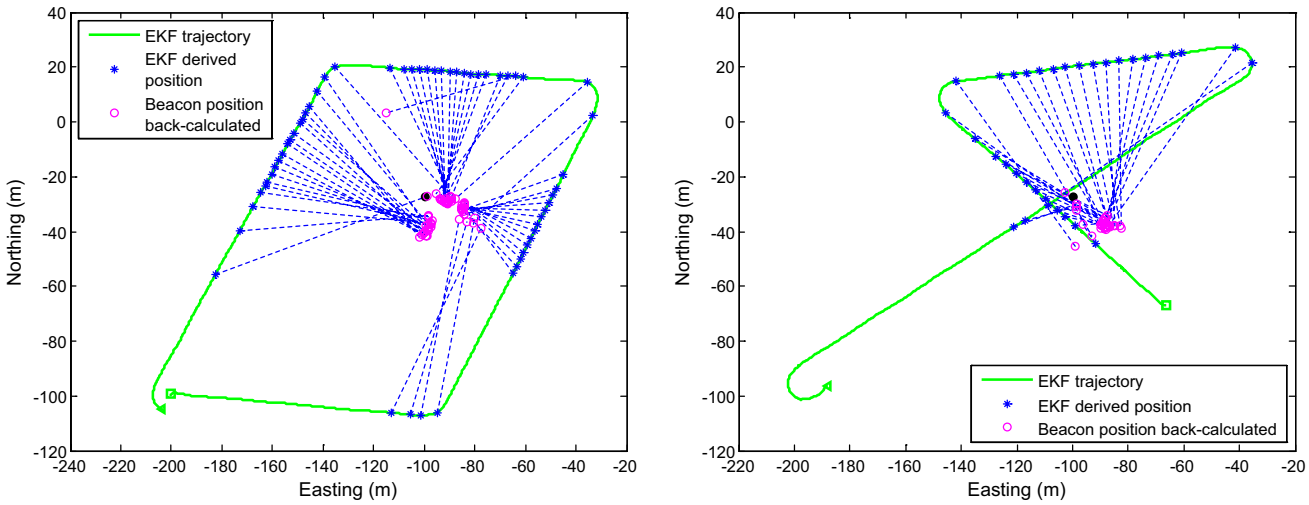

a Parallelogram trajectory

b Trajectory similar to the figure of eight

Fig. 10 EKF navigation results without integration of USBL position fix. Green triangle and square indicate the start and end points of the vehicle flight, respectively; black point in the middle denotes the position of acoustic beacon obtained by GPS; blue asterisk indicates AUV's current position derived by EKF when USBL position fix is available; magenta circle presents the position of acoustic beacon back-calculated using USBL position fix; blue dashed line shows the relation between 'USBL fix' and back-calculated beacon position. (Color figure online)

along the EKF trajectory; see the blue asterisks in Fig. 10. The position of acoustic beacon was roughly obtained by GPS, so that it cannot be taken as the position reference; moreover, the EKF-derived results were not accurate as the initial condition also came from GPS data. Thus, it was hard to evaluate the accuracy of USBL position fix from the view of intuitive comparison of AUV absolute position between different positioning means. Since the USBL position fix denotes the relative range between the USBL sonar and the acoustic beacon, we can inversely calculate the position of acoustic beacon using the USBL position fix, and evaluate the USBL positioning precision with the distribution of the back-calculated beacon position, as the magenta circles show in Fig. 10.

From the distribution of the magenta circles, we can find that the USBL sonar system can provide error-bounded position fix within the range of 100 m, with the maximum positioning error of less than 5 m for a fixed heading running. The USBL sampling interval was 3 s. However, not all the sampling points could provide valid position fix, especially when the beacon was out of the view of USBL sonar. Note that as the vehicle ran closer to the beacon, the amount of position fix got larger, while the positioning accuracy also increased. Nevertheless, it is obvious that the error-bounded positioning accuracy of USBL sonar system can hardly ensure a successful docking operation.

The reasons for the obvious positioning difference between the static and dynamic tests are analyzed. One important possibility is that the rotation calculation of USBL position fix from body-fixed frame to inertial frame has to get the vehicle's attitude information involved, which is measured by the electronic compass, so that the attitude accuracy has great effect on the accuracy of USBL position fix. Besides, the asynchronous sampling between the two devices also introduces the calculating error into USBL position fix transformation. Another possibility is that the vehicle's motion amplifies the effect of acoustic propagation and signal processing delays on USBL positioning results, so the dynamic motion compensation should be further considered to increase the accuracy of the USBL positioning data.

4 Vision terminal guidance method

Since the USBL navigation is effective for long-range homing with error-bounded positioning accuracy, the more accurate vision guidance is applied instead of USBL navigation for short-range docking. Some vision or optical guidance methods have been discussed in the previous studies. Cowen et al. propose a simple but effective underwater vehicle guidance scheme which is based upon an optical quadrant tracker which locks onto a visible light source located at the dock [8]. In [10], a vision-guided system is developed which consists of a Charge Coupled Device (CCD) camera and a set of lights mounted around the entrance of a docking station. Due to the complexity of the multi-light guidance source, this paper focuses on the discussion of image processing procedure to identify the dock by discriminating the shot images

of the guidance lights; besides, a signal processing technique to remove noise on the light images is also introduced. The vision positioning method using two cameras and four LED lights is adopted in [11]. In this paper, the switch algorithm between the monocular and binocular positioning methods is presented.

As is mentioned in Sect. 2, our docking system adopts a CCD camera and an underwater light for terminal vision guidance, which works when the range between the vehicle and the dock is within 25 m. The working principle is similar to the one discussed in Cowen et al. [8], but with different image processing method and guidance algorithm. In fact, a single light is insufficient for a single camera to determine their relative position relation. While with the premise that the USBL system can navigate the vehicle close to the dock centerline, a target tracking method similar to missile navigation is applicable for the AUV to track the dock entrance using a simple vision guidance system. The proposed vision system has the advantage of being easy to implement and effective for guidance. Although the more complicated vision system with two cameras or more lights can provide more guidance information with a better performance, as is presented in Park et al. [10] and Li et al. [11], it is at the expense of increased complexity of both the system configuration and the signal processing algorithm, while the robustness and effectiveness of those systems still need to be further verified.

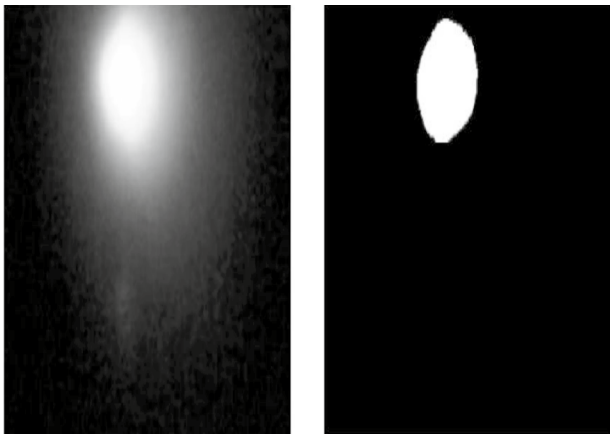

Fig. 11 Binarization processing of image

4.1 Vision guidance algorithm

In our study, the images shot by the camera are first processed by the DSP circuit for binarization; see Fig. 11. The location of the white pixels in the processed image implies the position of the dock light in the field-of-view of the vehicle camera. However, with a one-light and one-camera vision system, it is hard to obtain the relative position deviation between the vehicle and the dock centerline from the image information, but the relative deviation angles. The solved deviation angles can be compensated by vehicle attitude control (heading and pitch), which aims to make the origin of the image frame coincides with the center of the white pixels of the image [32].

Here, the 2-D image reference frame is fixed at the camera of the vehicle, while the center of the shot image is taken as the origin of the frame. The horizontal and vertical axes of the image frame are, respectively, denoted by Y and Z, which align with the $\boldsymbol{b}_2$ and $\boldsymbol{b}_3$ of the body-fixed frame, respectively; see Fig. 12. The average position of the white pixels is expressed by (y, z) in the image frame, with the unit of pixel, where $y, z \in [-255, 255]$. The coordinate values, respectively, indicate the left–right and up–down deviations of the vehicle with respect to the dock centerline. For an under-actuated AUV, the depth and cross-track errors are reduced indirectly by pitch and heading control, respectively. Based on the image information, the deviation angles α and β between the vehicle and the dock centerline can be calculated for vehicle attitude control, aiming to further reduce the depth and cross-track errors.

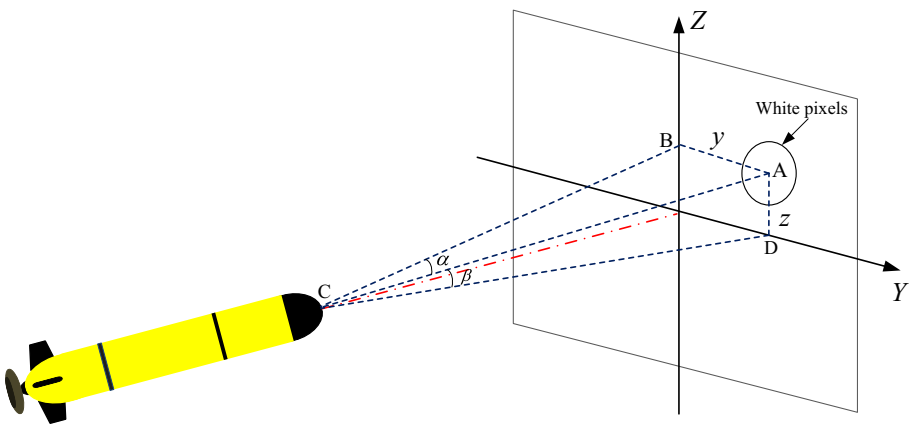

Fig. 12 Illustration of image interpretation

The viewing angle η of our camera is ranged from $-35°$ to 35°; for example, if $y = -255$, $\eta = -35°$, while if $y = 255$, $\eta = 35°$. Thus, the true distances denoted by y and z can be solved by trigonometric operations with the triangles ABC and ADC in Fig. 12, respectively:

$$\mathrm{AB} = \frac{y}{255} \cdot \tan(35°) \cdot \mathrm{BC},$$
$$\mathrm{AD} = \frac{z}{255} \cdot \tan(35°) \cdot \mathrm{DC}.$$

Then, the deviation angles α and βcan be calculated:

$$\alpha = \arctan\left(\frac{\mathrm{AB}}{\mathrm{BC}}\right) = \arctan\left(\frac{y}{255} \cdot \tan(35°)\right),$$
$$\beta = \arctan\left(\frac{\mathrm{AD}}{\mathrm{DC}}\right) = \arctan\left(\frac{z}{255} \cdot \tan(35°)\right).$$

Hence, the desired vision guidance angles for heading and pitch control are as follows:

$$\psi_{\mathrm{d}} = k_{\psi}\alpha,$$
$$\theta_{\mathrm{d}} = k_{\theta}\beta,$$

where k_{ψ} and k_{θ} are the control gains for effective guidance, which can be tuned by water trials.

To achieve successful docking operations, before the terminal docking attempt of the vehicle, some additional measures need to be taken to ensure that the vehicle could only dock with the dock entrance in the allowable directions. For example, taking the dock entrance orientation into consideration, the vehicle should be guided to arrive at the allowable area before the vision guidance system starts to work.

4.2 Docking experiments

The performance of vision terminal guidance is preliminarily validated by pool test; the experimental senario is similar to the pool test of USBL-based navigation, as discussed in Sect. 3.3.1. The main difference is that, for the first half of the flight, the vehicle runs with EKF navigation without integration of USBL position fix, while, for the last half of the flight, the vehicle approaches to the dock entrance under vision guidance; see Fig. 13. The vehicle starts from the opposite side of the dock with forward direction parallel to the dock centerline and different initial lateral deviations. The initial positions for EKF deviation are set separately for each docking mission. In Fig. 13, the EKF initial positions are indicated by the red points. The small spacing between two points is 1.25 m, while the large spacing between two points is 2.5 m.

Table 1 presents the experiment results of AUV docking operation with the combination of EKF navigation and vision guidance. AUV performed 14 times of docking operations in all, among which 2 cases were failed, and the left were successful. To simulate the USBL positioning error, the initial positions for EKF deviation were set different from the actual starting locations of the vehicle for most of the test cases. In such circumstances, the effectiveness

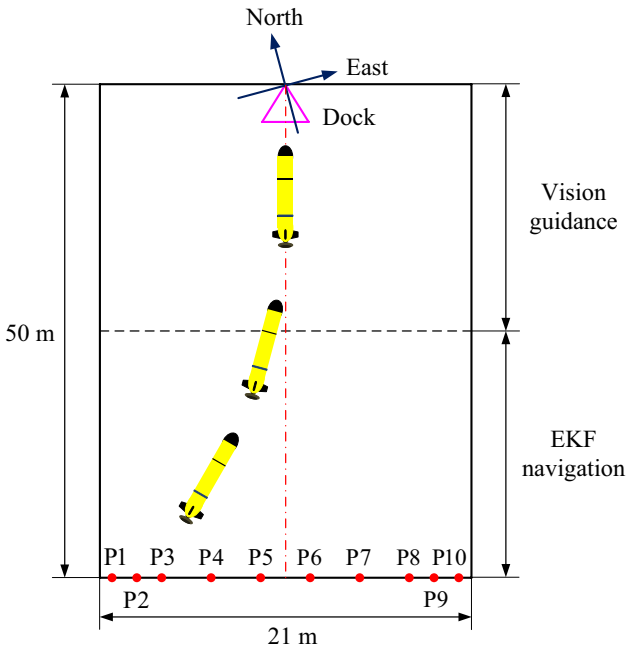

Fig. 13 Illustration of AUV docking operation with EKF navigation and vision guidance in the pool. The numbered red point indicates the different starting locations of the vehicle and the different initial positions for EKF deviation. The small spacing between two points is 1.25 m; the big spacing between two points is 2.5 m. (Color figure online)

Table 1 Docking experiment results under the combination of EKF navigation and vision guidance

Test number	AUV starting location	Initial position for EKF deviation	Result
1	P5	P5	Successful
2	P4	P5	Successful
3	P4	P5	Successful
4	P1	P1	Successful
5	P6	P5	Successful
6	P6	P5	Successful
7	P3	P5	Successful
8	P3	P5	Successful
9	P2	P5	Successful
10	P2	P5	Successful
11	P1	P5	Failed
12	P9	P6	Successful
13	P10	P6	Successful
14	P10	P6	Failed

of vision guidance system can be fully demonstrated. The experimental results indicated that the maximum position-error tolerance of vision guidance could be at least 6.25 m, according to the test cases No. 9, No. 10, and No. 12 in Table 1.

The pool test was implemented at night to make sure that the vision system could work well. Figure 14 presents the time-series photos of one successful docking operation. It can be found that there were some light reflections on the surface of water, which came from the surrounding environment; however, they actually did not cause any disturbance throughout the docking operations, as the camera only shot the scenes forward. While the real disturbance was the light reflection on the side wall of the pool, coming from the strobe light located on the back of the vehicle, which is used for vehicle identification. When the AUV was "deceived" to start close to the side wall which meaned that the initial position for EKF derivation was different from the vehicle's true position, such as the test cases No. 11 and No. 14, the vehicle ran along the side wall and attracted by its own reflection before finding the true light for docking guidance. This caused the failure of the two docking attempts. Therefore, the maximum position-error tolerance of vision guidance still needs to be further confirmed due to the size limitation of the pool. Nevertheless, the EKF navigation accuracy with the integration of USBL position fix is able to meet the positioning demand of vision terminal guidance to ensure successful docking operation.

The presented vision system is selected due to its low complexity and low cost, but effective performance. The experimental results with the vehicle docking on the water surface showed that the environmental lights could cause obvious disturbances during AUV docking process, which reflected the performance limitation of our vision guidance system. However, this limitation depends on the specific application environment. In the real applications, the dock station could be located on the sea floor at over 50 m water depth, where it will be dark with less optical disturbance from the surroundings. Nevertheless, it is still necessary to improve our vision guidance system to avoid the potential risks. In order not to increase too much of the system complexity, adding more identifiable features to the light source will be taken into consideration.

5 Conclusions

An underwater AUV docking system was briefly introduced in this paper. Due to the performance features of the existing underwater navigation techniques, the combination of USBL-based navigation and vision guidance was adopted for the AUV to perform docking missions.

USBL sonar system has the advantage of homing the vehicle to the dock station in long range. An integrated navigation algorithm based on EKF was proposed for AUV navigation. The outlier rejection issue was carefully addressed to make sure that the EKF algorithm could be properly applied. The software of navigation algorithm was implemented based on MOOS-IvP. The performance of the proposed navigation system was validated by pool and lake tests, respectively. Although USBL-based navigation method had effective capability of homing the vehicle close to the dock station, it can hardly navigate the vehicle entering the dock entrance with its error-bounded positioning accuracy.

While, for short-range docking, the more accurate vision guidance method was applied instead of USBL navigation.

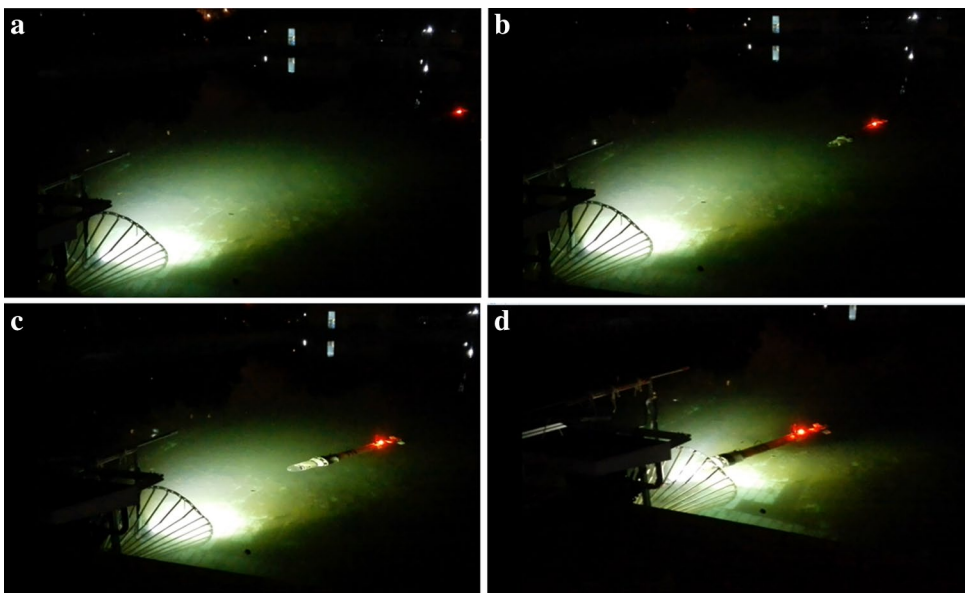

Fig. 14 Successful docking operation

The simple but effective vision guidance system and algorithm were discussed. Docking experiments in the pool environment were conducted to validate the combined performance of EKF navigation and vision guidance. The experimental results demonstrated the effectiveness of the vision system for terminal guidance, with the maximum position-error tolerance of at least 6.25 m. Ongoing research will focus on the accuracy enhancement of USBL positioning results as well as the improvement of vision system to avoid the misleading of environmental lights, such as adding more identifiable features to the light source. In addition, sea trials will be further conducted to investigate the effectiveness and reliability of our docking system and the complete docking scheme.

Acknowledgements The authors would like to thank for the sustained effort of the entire AUV docking team, including Jia Mao, Tongchen Wang, Rui Yu, Tao Zhang, Junyou Zhang, and Mingwei Lin. This work is partly supported by National High Technology Research and Development Program of China (no. 2013AA09A414), China Postdoctoral Science Foundation (no. 2015M571869), and Open Fund of Hangzhou Dianzi University.

References

1. McEwen RS, Hobson BW, McBride L, Bellingham JG (2008) Docking control system for a 54-cm-diameter (21-in) AUV. IEEE J Ocean Eng 33(4):550–562
2. Singh H, Bellingham JG, Hover F, Lerner S, Moran BA, von der Heydt K, Yoerger D (2001) Docking for an autonomous ocean sampling network. IEEE J Ocean Eng 26(4):498–514
3. Stokey R, Allen B, Austin T, Goldsborough R, Forrester N, Purcell M, von Alt C (2001) Enabling technologies for REMUS docking: an integral component of an autonomous ocean-sampling network. IEEE J Ocean Eng 26(4):487–497
4. Guo J (2008) Mooring cable tracking using active vision for a biomimetic autonomous underwater vehicle. J Mar Sci Technol 13(2):147–153
5. Maki T, Mizushima H, Ura T, Sakamaki T, Yanagisawa M (2012) AUV navigation around jacket structures I: relative localization based on multi-sensor fusion. J Mar Sci Technol 17(17):330–339
6. Maki T, Ura T, Sakamaki T (2012) AUV navigation around jacket structures II: map based path-planning and guidance. J Mar Sci Technol 17(4):523–531
7. Teo K, Goh B, Chai OK (2015) Fuzzy docking guidance using augmented navigation system on an AUV. IEEE J Ocean Eng 40(2):349–361
8. Cowen S, Briest S, Dombrowski J (1997) Underwater docking of autonomous undersea vehicles using optical terminal guidance. In: Proceedings of MTS/IEEE OCEANS conference, Halifax, NS, USA, vol 2, pp 1143–1147
9. Park J, Jun B, Lee P, Lee F, Oh J (2007) Experiment on underwater docking of an autonomous underwater vehicle 'ISiMI' using optical terminal guidance. In: Proceedings of MTS/IEEE OCEANS conference, Aberdeen, UK, pp 1–6
10. Park J, Jun B, Lee P, Oh J (2009) Experiments on vision guided docking of an autonomous underwater vehicle using one camera. Ocean Eng 36:48–61
11. Li Y, Jiang Y, Cao J, Wang B, Li Y (2015) AUV docking experiments based on vision positioning using two cameras. Ocean Eng 110:163–173
12. Feezor MD, Sorrell FY, Blankinship PR, Bellingham JG (2001) Autonomous underwater vehicle homing/docking via electromagnetic guidance. IEEE J Ocean Eng 26(4):515–521
13. Kronen D (1997) Docking the ocean explorer autonomous underwater vehicle using a low cost acoustic positioning system and a fuzzy logic guidance algorithm. M.S. thesis, Department of Ocean Engineering, Florida Atlantic University, Dania Beach, FL, USA.
14. Smith SM, Kronen D (1997) Experimental results of an inexpensive short baseline acoustic positioning system for AUV navigation. In: Proceedings of MTS/IEEE OCEANS conference, Halifax, NS, USA, vol 1, pp 714–720
15. Allen B, Austim T, Forrester N, Goldsborough R, Kukulya A, Packard G, Purrell M, Stokey R (2006) Autonomous docking demonstrations with enhanced REMUS technology. In: Proceedings of MTS/IEEE OCEANS conference, Boston, MA, USA, pp 1–6
16. Lefebvre T, Bruyninckx H, De Schutter J (2004) Kalman filters for non-linear systems: a comparison of performance. Int J Control 77(7):639–653
17. Kushner HJ (1967) Dynamical equations for optimum nonlinear filtering. J Differ Equ 26(3):179–190
18. Simon D (2006) Optimal state estimation. Wiley, Hoboken
19. Arasaratnam I, Haykin S, Hurd TR (2010) Cubature Kalman filtering for continuous-discrete systems: theory and simulations. IEEE Trans Signal Process 58(10):4977–4993
20. Zhang M, Xu Y, Li B, Wang D, Xu W (2014) A modular autonomous underwater vehicle for environmental sampling: system design and preliminary experimental results. In: Proceedings of MTS/IEEE OCEANS conference, Taipei, pp 1–5
21. Li D, Chen Y, Shi J, Yang C (2015) Autonomous underwater vehicle docking system for cabled ocean observatory network. Ocean Eng 109:127–134
22. https://www.evologics.de/en/products/USBL/s2cr_18_34_usbl.html. Accessed 2017
23. http://www.outlandtech.com/cameras/UWC-325-SS-Color-Camera. Accessed 2017
24. Yang C, Peng S, Fan S (2016) Study on docking guidance algorithm for hybrid underwater glider in currents. Ocean Eng 125:170–181
25. Kalman RE (2001) Control theory: twenty-five seminal papers (1932–1981). Wiley-IEEE Press, Hoboken, pp 147–166
26. Fossen TI (1995) Guidance and control of ocean vehicles. Wiley, Chichester
27. Vaganay J, Leonard JJ, Bellingham JG (1996) Outlier rejection for autonomous acoustic navigation. In: Proceedings of IEEE international conference on robotics and automation, Minneapolis, MN, USA, vol 3, pp 2174–2181
28. Qin Y, Zhang H, Wang S (2012) Kalman filter and principle of integrated navigation. Northwestern Polytechnical University Press, Xi'an
29. Newman PM (2003) MOOS—a mission orientated operating suite. Massachusetts Institute of Technology, Technical Report 2003-07
30. Benjamin MR, Leonard JJ, Schmidt H, Newman PM (2009) An overview of MOOS-IvP and a brief users guide to the IvP Helm autonomy software. Massachusetts Institute of Technology, Technical Report 2009-028
31. http://www.moos-ivp.org. Accessed 2017
32. Li B, Xu Y, Liu C, Fan S (2015) Terminal navigation and control for docking an underactuated autonomous underwater vehicle. In: Proceedings of IEEE international conference on cyber technology in automation, control, and intelligent systems, Shenyang, Zhejiang, China, pp 25–30